RSC Advances

PAPER

View Article Online
View Journal | View Issue

Cite this: *RSC Adv.*, 2019, **9**, 35924

An efficient and thermally stable dye-sensitized solar cell based on a lamellar nanostructured thiolate/disulfide liquid crystal electrolyte and carbon/PEDOT composite nanoparticle electrode†

Caihong Wang, Xueyong Li, Yong Wu and Shuai Tan *

A thiolate/disulfide redox based lamellar nanostructured smectic liquid crystal electrolyte with an optimized configuration and a carbon/PEDOT composite nanoparticle electrode were prepared for efficient dye-sensitized solar cells (DSSCs). The configuration of the optimized electrolyte consisted of 1-dodecyl-3-methyl-1*H*-imidazol-3-ium 1-methyl-1*H*-tetrazole-5thiolate/di-5-(1-methyltetrazole) disulfide/TBP/$LiClO_4$ in the molecular ratio of 2 : 1 : 1 : 0.1. The carbon/PEDOT composite electrode was developed by electrochemical deposition of PEDOT on a carbon nanoparticle electrode. The additives in the lamellar nanostructured electrolyte were revealed to lower the viscosity of the electrolyte for promoted ion diffusion, as well as benefit the charge transfer process in the DSSC. The carbon/PEDOT nanoparticle electrode was suggested to provide improved catalytic activity and large surface area to favor the charge transfer at the cathode/electrolyte interface of the DSSC. As a result, the DSSC fabricated using the optimized smectic electrolyte, the composite nanoparticle electrode, together with a Z907 sensitized photoanode, attained a maximum power conversion efficiency of 6.5% at 40 °C and stable efficiencies higher than 6.0% within a temperature range from 35 to 55 °C. These results show potential of the optimized smectic thiolate/disulfide electrolyte based DSSCs operating efficiently and stably under outdoor conditions.

Received 3rd September 2019
Accepted 1st November 2019

DOI: 10.1039/c9ra07043e

rsc.li/rsc-advances

1. Introduction

Dye-sensitized solar cells (DSSCs) have attracted intensive interest due to their desirable properties such as good performance in diverse light conditions, low production cost and easy fabrication.[1–3] Typically, a DSSC consists of three fundamental components: a dye-sensitized working electrode (WE), a counter electrode (CE), and an electrolyte containing redox couples. The electrolyte sandwiched between the WE and CE is responsible for the inner charge transport between electrodes and continuously regenerates the dye and itself at the interface.[4] To date, the iodide/triiodide (I^-/I_3^-) redox couple has been widely used in the electrolyte, achieving a conversion efficiency up to 12% for the global AM1.5 spectrum.[5] However, due to the shortcomings of the I^-/I_3^- redox couple such as corrosion of the metal CE and absorption of visible light, many attempts have been invested to find alternative redox couples to replace the ubiquitous I^-/I_3^- system.[6–9] An organic thiolate/disulfide (T^-/T_2) redox couples with noncorrosive and transparent nature, as well as acceptable efficiency have drawn attention as promising alternative mediators for DSSC applications.[9–11] Wang *et al.* firstly employed tetramethylammonium T^-/T_2 in acetonitrile/ethylene carbonate as electrolytes for DSSCs, resulting in a power conversion efficiency (PCE) of 6.4%.[9] Considering the leakage and volatilization of the liquid electrolytes, developing solvent-free T^-/T_2 electrolytes with high PCE is desirable for cell stability and longevity.[4]

Ionic liquid crystals have shown potential as electrolytes due to the dynamically ordered molecular arrangements for charge transport and non-volatile property for improving both the efficiency and the long-term stability of DSSC for outdoor conditions.[12–16] Previously, we reported an ionic liquid crystal electrolyte consisting of smectic [C_{12}MIm][T] (1-dodecyl-3-methyl-1*H*-imidazol-3-ium 1-methyl-1*H*-tetrazole-5thiolate) and T_2 (di-5-(1-methyltetrazole) disulfide) and equipped a DSSC with a Pt CE and a Z907-sensitized WE.[16] The lamellar arrangement of the smectic T^-/T_2 redox couple was revealed to improve the Grotthuss-type charge transport and suppress the electron recombination in DSSCs. The PCE of the corresponding DSSC increased with the increase in temperature and reached 4.1% at 70 °C. Despite the stable performance at elevated temperatures, the PCE of the T^-/T_2 liquid crystal electrolyte based DSSC needs to be further improved for practical applications due to the low

School of Chemical Engineering, Sichuan University, No. 24 South Section 1, Yihuan Road, Chengdu 610065, China. E-mail: tanshuai@scu.edu.cn

† Electronic supplementary information (ESI) available: DSC measurements, POM observations, SAXS analyses, volatile, cyclic voltammetry measurements of the electrolytes, images of the electrodes and DSSCs, and SEM image of the carbon electrode. See DOI: 10.1039/c9ra07043e

fill factor (FF, about 0.47 at 40 °C) and relatively low short-circuit current density (J_{sc}, about 10 mA cm^{-2} at 40 °C). It was suggested that the commonly used Pt CE shows poor electrocatalytic activity for disulfide reduction, leading to the low FF and J_{sc} of the T^-/T_2 based DSSC.[17] Various electrodes including carbon materials,[18–22] PEDOT (poly(3,4-ethylenedioxythiophene)),[23–25] or transition metal compounds[25–28] have been proposed as promising CE for DSSCs. Additionally, electrical additives, such as 4-*tert*-butylpyridine (TBP) or lithium ions, are substantial component in the electrolytes for optimizing the photovoltaic performance.[4] However, the alternative electrodes and the additives have yet to be employed for the liquid crystal electrolyte based DSSCs.

With a view to further improving the performance of the T^-/T_2 liquid crystal electrolytes in DSSCs, a smectic T^-/T_2 electrolyte with an optimized configuration containing $[C_{12}MIm][T]/T_2$/TBP/$LiClO_4$ in the molar ratio of 2 : 1 : 1 : 0.1 was prepared, and a carbon/PEDOT composite nanoparticle CE was adopted instead of Pt electrode for DSSC fabrication. The introduction of the additives in the lamellar T^-/T_2 nanostructures lowered the viscosity to promote the ion diffusion in the electrolyte and favoured the overall charge transfer process in the DSSCs. Meanwhile, the carbon/PEDOT nanoparticle CE provided improved catalytic activity and large surface area for T^-/T_2 redox to benefit the charge transfer process at the CE/electrolyte interface in DSSC. As a result, the FF, J_{sc} and open-circuit voltage (V_{oc}) of the DSSCs derived from the optimized electrolyte and the carbon/PEDOT composite CE were greatly enhanced and an optimized PCE value of 6.5% was obtained at 40 °C, which was increased by 100% than that of pure $[C_{12}MIm][T]/T_2$ and Pt CE based DSSCs. The derived DSSC maintained relatively stable photovoltaic performance with PCE higher than 6.0% within a temperature range from 35 to 55 °C. The appreciable thermal stability and efficiency reveals the great potential of organic liquid crystal electrolytes based DSSCs towards practical application.

2. Experimental

2.1 Materials

All commercially-available starting materials, reagents and solvents were used as supplied and were obtained from TCI and Acros. The carbon ink (Advanced Carbonic Ink 234) was purchased from Shanghai Ink Factory as the source of the carbon material for CE preparation and used as supplied without further purification. $[C_{12}MIm][T]$ and T_2 were prepared according to the procedures described previously.[9,16]

2.2 Characterization

Polarized optical micrographs of the samples were observed using a Weitu XPL-30TF polarizing optical microscope (POM) equipped with a WT-3000 hot-stage. The differential scanning calorimetry (DSC) measurements were performed by a TA DSC Q20 modulated instrument at a heating rate of 10 °C min^{-1}. The small angle X-ray scattering (SAXS) analyses were carried out by an Anton Paar SAXSess mc^2 high flux small angle X-ray scattering instrument equipped with a Kratky block-collimation system and an image plate detector, using Cu-Kα radiation at 40 kV and 50 mA. Sample's temperature was controlled by a hot-stage. The Ultraviolet-visible (UV-Vis) absorption spectra were obtained with a Shanghaiyidian L5 UV-Vis spectrophotometer. The electrolyte was 1000 times diluted in methanol solution before UV-Vis absorption measurement. The temperature dependent viscosity of the electrolytes was determined using a TA instrument AR2000 rotational rheometer. The scanning electron microscope (SEM) observations and the energy dispersive X-ray spectroscopies (EDS) of the electrodes were performed by a Nova NanoSEM450 field emission SEM equipped with an EDS detector at an accelerating voltage of 5 kV. The photocurrent–voltage (J–V) measurements were performed on a PEC-S20 action spectrum measurement setup under AM1.5G solar light (100 mW cm^{-2}) simulated by a Pecell-L15 solar simulator calibrated using a certified BS-520 C–Si solar cell. The impedance spectra of electrochemical impedance spectroscopy (EIS, Frequency range: 100 kHz to 0.01 Hz) and CV (scanning rate: 10 mV s^{-1}) measurements were recorded on an EG&G Princeton Applied Research P4000+ workstation connected to a PC running electrochemical impedance software. The EIS measurements of the DSSCs were conducted at the bias voltage of −0.6 V under open-circuit condition at dark environment, while the EIS measurements of the symmetric cell were performed with no bias voltage. Diffusion coefficient (D) of the electrolyte was determined from the limited current (J_{lim}) obtained by CV measurement using a symmetric cell. A hot-stage with a clamp was used to fix the device and control the sample's temperature for the electrochemical measurements. The device was heated to the certain temperature and kept for 5 min before each measurement.

2.3 Electrolyte preparation

TBP and $LiClO_4$ were simultaneously applied as additives for smectic T^-/T_2 electrolyte preparation due to their different mechanisms on optimizing the photovoltaic performance of DSSCs.[4] The $[C_{12}MIm][T]$, T_2, TBP and $LiClO_4$ with a molar ratio of 2 : 1 : 1 : 0.1 were dissolved in chloroform/methanol (3 : 1 volume ratio). The solution was stirred for 30 min, and then the solvent was removed under reduced pressure to give a homogeneous additive doped electrolyte ($C_{12}T_{add}$). The prepared electrolyte $C_{12}T_{add}$ showed negligible absorption of visible light, as shown in Fig. 1. An additive-free electrolyte ($C_{12}T$) composed of $[C_{12}MIm][T]$ and T_2 with molar ratio of 2 : 1 was also prepared as a reference.

2.4 Electrode preparation and DSSC fabrication

The photoanode was prepared by screen printing TiO_2 film (0.4 cm × 0.4 cm) on a fluorine-doped tin oxide (FTO) glass substrate as described in the literature.[9] An 8 μm thick layer of 20 nm-sized TiO_2 particles was first printed on the substrate and a 5 μm thick scatting layer of 400 nm-sized TiO_2 particles was further coated. The sintered TiO_2 electrode was immersed into a 0.2 mM ethanol solution of the Z907Na sensitizer for 20 h. The active area of the photoanode was 0.16 cm^2.

The carbon/PEDOT composite nanoparticle CE was prepared as follow. The carbon ink was spin-coated on a FTO glass

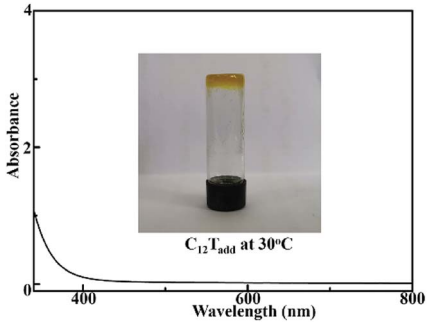

Fig. 1 Ultraviolet-visible absorption spectrum of $C_{12}T_{add}$ in methanol and image of $C_{12}T_{add}$ at 30 °C.

substrate at 2000 rpm for 1 min, then the substrate was baked at 200 °C for 30 min to obtain a carbon electrode. The carbon/PEDOT composite electrode was further prepared by electrochemical polymerization of 3,4-ethylenedioxythiophene (EDOT) monomer on the carbon electrode *via* cyclic voltammetry (CV) technology using a three-electrode system.[20] The working electrode, the counter electrode and the reference electrode in the three-electrode system were the carbon electrode, a freshly polished Pt foil electrode and an aqueous Ag/AgCl reference electrode, respectively. The electrolyte for EDOT polymerization was composed of 0.1 mol L^{-1} lithium bis(trifluoromethanesulfonyl) imide and 0.02 mol L^{-1} EDOT in acetonitrile. The applied voltage range of CV for EDOT polymerization was −0.4 V to 1.2 V with a scan rate of 10 mV s^{-1}. After that, the composite electrode was baked at 85 °C for 20 min. The carbon/PEDOT composite CE and pure carbon CE were non-transparent, as shown in ESI Fig. 4a.† A Pt CE was also prepared as reference by thermal decomposition method as described in the literature.[29]

The appropriate amount of the prepared electrolyte (3–5 mg) was sandwiched between the photoanode and CE and then sealed with a hot-melt Surlyn at 70 °C. The DSSCs equipped with carbon/PEDOT composite CE and $C_{12}T_{add}$ electrolyte, carbon/PEDOT composite CE and $C_{12}T$ electrolyte, carbon CE and $C_{12}T_{add}$ electrolyte, and Pt CE and $C_{12}T_{add}$ electrolyte were denoted as CP-$C_{12}T_{add}$, CP-$C_{12}T$, C–$C_{12}T_{add}$ and Pt–$C_{12}T_{add}$, respectively. The images of the prepared DSSCs are shown in ESI Fig. 4b.†

3. Results and discussion

3.1 Impact of additives on liquid crystal electrolytes

As we reported previously, $C_{12}T$ exhibited smectic A (S_A) phase from 12.5 to 75.5 °C.[16] After doping with the additives, the liquid crystal mesophase preserved in $C_{12}T_{add}$. DSC measurements, POM observations and SAXS analyses (see the ESI†) confirmed the presence of the S_A phase of $C_{12}T_{add}$ over a temperature range from 0 to 51 °C and a lamellar structure with an interlayer spacing of 3.29 nm formed in smectic $C_{12}T_{add}$. These results suggested that $C_{12}T_{add}$ formed lamellar nanostructures in the smectic phase, as shown in inset of ESI Fig. 1b,† which could assemble layered pathways for efficient charge transport.[16]

In order to further clarify the impact of doped additives on the liquid crystal electrolytes, temperature dependent viscosities (μ) of the liquid crystal electrolytes were determined by rotational rheometer. As shown in Fig. 2a, the viscosities of $C_{12}T_{add}$ were greatly lowered after doping the liquid TBP and $LiClO_4$ in $C_{12}T$. Despite a relatively low viscosity, $C_{12}T_{add}$ was still too viscous to flow at room temperature (inset of Fig. 1) and non-volatile at 40 °C for 48 h under vacuum condition (see the ESI†). Since the charge diffusion in the electrolytes is related to the viscosity, the lowered viscosity would favor the charge diffusion. Temperature dependent diffusion coefficients (D_T) of $C_{12}T_{add}$ were further characterized by CV measurements (see the ESI†) using a symmetric thin-film setup as described in the literature.[30] As shown in Fig. 2b, the obtained D_T increased with the increase in temperature for both the smectic electrolytes and the log D_T was approximately linearly dependent on T^{-1}. D_T decreased by 15% at the S_A phase to isotropic liquid phase transition point for $C_{12}T_{add}$, which indicated the beneficial effect of lamellar nanostructures on the charge transport. By doping with the additives, the charge diffusion coefficient of lamellar nanostructured $C_{12}T_{add}$ were greatly improved compared with the undoped $C_{12}T$. Meanwhile, the slope of log D_T *versus* T^{-1} for smectic $C_{12}T_{add}$ was much lower than that for smectic $C_{12}T$, suggesting a lower activation energy for charge transport in $C_{12}T_{add}$. These results indicated that the introduced additives favoured the charge diffusion in lamellar T^{-}/T_2 nanostructures.

3.2 The morphology of the CEs

The morphologies of the prepared carbon/PEDOT composite CE and pure carbon CE were revealed by SEM observations (ESI

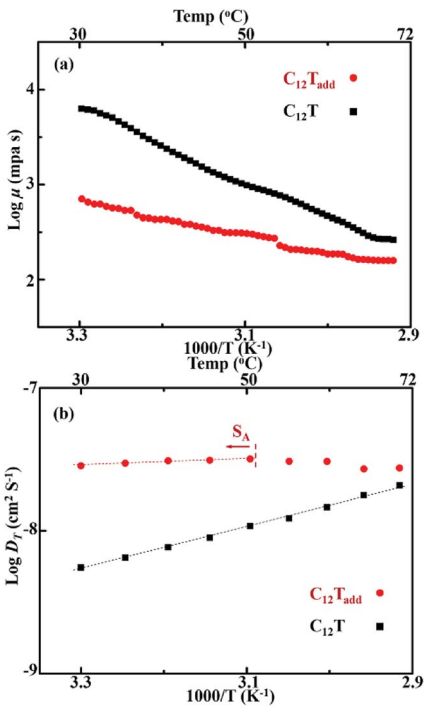

Fig. 2 Temperature dependent μ (a) and D_T (b) of $C_{12}T_{add}$ and $C_{12}T$.

Fig. 3† and 3). As shown in ESI Fig. 3a,† the morphology of the coated carbon electrode exhibited spherical nanoparticular structures on the FTO substrate with an average diameter of about 35 nm. This result suggested that the carbon CE could provide a high surface area for charge transfer at the interface between the CE and the electrolyte in DSSCs. Although the carbon was an alternative CE material comparative to Pt due to the abundance, low cost and high electrical conductivity and catalytic surface area,[31] the carbon electrode could to be further optimized for the T^-/T_2 systems for high efficient DSSCs due to the relatively slow kinetics of the electrochemical reaction and insufficient electrocatalytic activity.[20–23] PEDOT is also an alternative CE material with excellent electrocatalytic activity towards the T^-/T_2 mediator.[23,25] However, the conductivity of PEDOT electrode *via* spin coating is relatively low for the application in DSSCs.[32] In view of these, we employed the advantages of carbon and PEDOT materials and prepared the carbon/PEDOT composite electrode for the smectic T^-/T_2 based DSSC *via* spin coating and electrochemical polymerization deposition method. For the carbon/PEDOT composite electrode (Fig. 3), the carbon nanoparticles provided considerable surface area for PEDOT deposition and the PEDOT was homogeneously attached to the carbon nanoparticles to form carbon/PEDOT composite nanoparticle electrode on the FTO substrate. The EDS mapping image (ESI Fig. S6†) of the carbon/PEDOT composite nanoparticle electrode revealed the uniform distribution of sulfur atom, which indicated the successful electrochemical polymerization of EDOT monomer on the carbon electrode. The thickness of the carbon/PEDOT nanoparticle layer was uniform with a size of about 800 nm (Fig. 3a). The average diameter of the carbon/PEDOT composite nanoparticle was around 40 nm (Fig. 3b). The square resistances of the prepared carbon electrode and carbon/PEDOT composite electrode were about 27 and 35 Ω cm^{-2}, respectively.

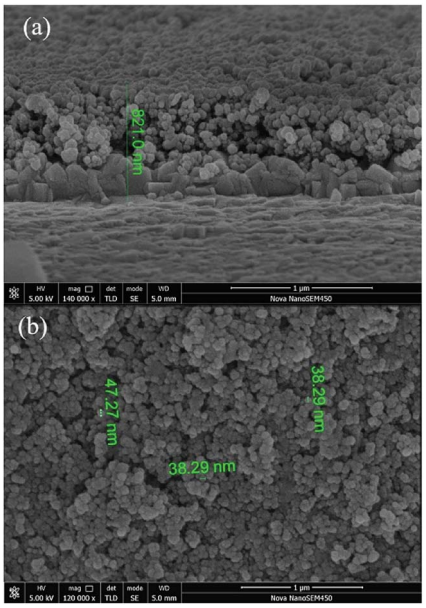

Fig. 3 SEM images of the carbon/PEDOT composite CE: (a) cross-section, (b) top surface.

3.3 Photovoltaic performance of DSSCs

The photovoltaic performance of the prepared DSSCs were evaluated by *J–V* measurements under simulated AM1.5G solar light (100 mW cm^{-2}). The *J–V* curves of the DSSCs at 30 °C are shown in Fig. 4. The J_{sc}, V_{oc}, FF and PCE of the DSSCs obtained from the *J–V* curves are listed in Table 1. The C–$C_{12}T_{add}$ and Pt–$C_{12}T_{add}$ exhibited considerable J_{sc} (>14 mA cm^{-2}) and V_{oc} (about 0.62 V). The J_{sc} of C–$C_{12}T_{add}$ was higher than that of Pt–$C_{12}T_{add}$, which was probably due to a larger surface area. However, both the cells suffered from low FF (<0.5), resulting in a limited PCE. Introducing PEDOT layers between the carbon nanoparticles and the electrolyte led to a desirable improvement in FF for CP-$C_{12}T_{add}$. The improved FF indicated the introduced PEDOT layers favoured the charge transfer process at the CE/electrolyte interface. At 30 °C, the J_{sc}, V_{oc}, FF and PCE of CP-$C_{12}T_{add}$ were 15.8 mA cm^{-2}, 0.642 V, 0.568 and 5.76%, respectively. TBP and $LiClO_4$ were reported as effective additives capable of enhancing the photovoltaic performance of DSSCs.[4] By comparing the photovoltaic performance of CP-$C_{12}T_{add}$ and CP-$C_{12}T$, the presence of the additives in the liquid crystal electrolyte produced a remarkable increase in overall photovoltaic parameters for CP-$C_{12}T_{add}$, resulting in an improvement of PCE from 3.83% to 5.76%. The impacts of the additives and the electrodes on the improved performance for the liquid crystal electrolyte based DSSCs were further analyzed by EIS measurement, which was discussed in Section 3.4.

Typically, DSSCs based on commonly used electrolytes would suffer from deteriorated efficiency at elevated temperatures, which is one of the most challenging issues in solar cell technology.[33] Nevertheless, liquid crystal electrolytes possess non-volatile and thermally stable properties, which have shown advantages in DSSCs at elevated temperatures.[14–16] In order to evaluate the temperature dependent performance of the smectic $C_{12}T_{add}$ based DSSC, photovoltaic characterization of CP-$C_{12}T_{add}$ was further performed during the heating process from 30 to 60 °C. The obtained J_{sc}, V_{oc}, FF and PCE are presented in Fig. 5. The J_{sc} of CP-$C_{12}T_{add}$ (Fig. 5a) increased with increasing temperature and reached the maximum of 17.1 mA cm^{-2} at 45 °C. After that, the J_{sc} decreased from 50 to 60 °C due to the absence of the lamellar nanostructures. The V_{oc} of CP-$C_{12}T_{add}$ (Fig. 5b) decayed from 0.644 V to 0.570 V during heating the cell from 30 to 60 °C, while the FF of CP-

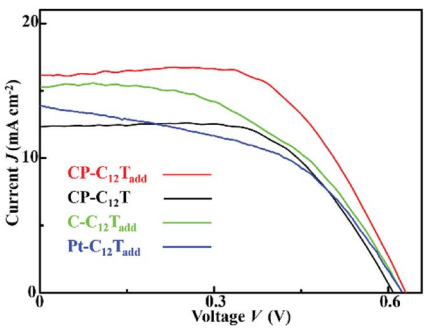

Fig. 4 *J–V* curves of CP-$C_{12}T_{add}$, CP-$C_{12}T$, C–$C_{12}T_{add}$ and Pt–$C_{12}T_{add}$ at 30 °C.

Table 1 J_{sc}, V_{oc}, FF and PCE of the DSSCs obtained from J–V curves and R_{CE} from EIS measurements at 30 °C

DSSC	J_{sc} (mA cm^{-2})	V_{oc} (V)	FF	PCE	R_{CE}[a] (Ω cm^{-2})
Pt–$C_{12}T_{add}$	14.0	0.621	0.455	3.96%	88
C–$C_{12}T_{add}$	15.1	0.621	0.488	4.57%	60
CP-$C_{12}T_{add}$	15.8	0.642	0.568	5.76%	29
CP-$C_{12}T$	11.8	0.617	0.527	3.83%	38

[a] Calculated from the half resistance value of the EIS fitting multiplied by the geometric surface area of the symmetric cell.

$C_{12}T_{add}$ (Fig. 5c) increased from 0.568 to 0.624. The temperature dependence of the photovoltaic parameters for CP-$C_{12}T_{add}$ was in consistent with that of the reported liquid crystal electrolyte based DSSCs.[15,16] Owing to the optimization on the electrolyte and CE, CP-$C_{12}T_{add}$ achieved a maximum PCE of 6.5% at 40 °C, which was enhanced by 100% than that of pure [C_{12}MIm][T]/T_2 and Pt CE based DSSCs at the same temperature.[16] To the best of our knowledge, this was the highest PCE achieved by liquid crystal electrolyte based DSSCs. Notably, the CP-$C_{12}T_{add}$ maintained relatively stable photovoltaic performance with PCE higher than 6.0% within a temperature range from 35 to 55 °C, which have great potential for operating at outdoor conditions.

3.4 Impact of CE and additives on the DSSC interfaces

EIS measurements were applied to analysis the impact of the additives and CE on the DSSC interfaces between the electrodes and electrolyte. Symmetric cells (inset of Fig. 6) were firstly employed to reveal the impact of additives and CE on the CE/electrolytes interface.[34] The Nyquist plots of the symmetric cells obtained from EIS measurements at 0 V bias potential under 30 °C are shown in Fig. 6. On the basis of EIS theory, the ideal Nyquist plot of the symmetric cell should compose of a semicircle at high frequency due to the charge transfer at the electrode/electrolyte interface and a Warburg impedance caused by ion diffusion through the electrolyte at the medium frequency.[34] This ideal spectrum was observed in the case of

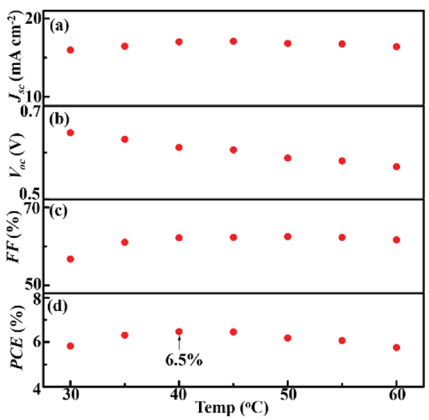

Fig. 5 Temperature dependent J_{sc} (a), V_{oc} (b), FF (c) and PCE (d) of CP-$C_{12}T_{add}$.

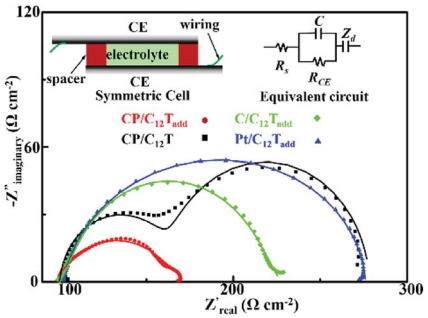

Fig. 6 Nyquist plots of the symmetric cells with various CEs obtained from EIS measurements at 30 °C (discrete symbols: experimental results, solid lines: fitted data, inset is the equivalent circuit).

the symmetric cells based on composite electrode and liquid crystal electrolytes. However, the Warburg impedance was undetected during the measured frequency for the Pt electrode and pure carbon electrode based cells. Similar phenomenon was also observed for the reported DSSCs with T^-/T_2 and Pt systems.[22] The charge transfer resistance (R_{CE}, Ω cm^{-2}) at the electrode/electrolyte interface was calculated from the half resistance value of the EIS fitting multiplied by the geometric surface area of the symmetric cell and listed in Table 1. Obviously, the R_{CE} value of the carbon/PEDOT electrode is much lower than that of the Pt electrode and pure carbon electrode, indicating an improved charge transfer process between the carbon/PEDOT electrode and $C_{12}T_{add}$. Another important parameter in the EIS characterization is the frequency of the characteristic response peaks in the high frequency region of the Bode plot, signifying the electron transfer rate at the electrode/electrolyte interface. The frequency of the characteristic response peak (listed in Fig. 6) for the carbon/PEDOT electrode was much higher than that of the Pt electrode and pure carbon electrode, revealing a faster electron transfer rate at the interface of carbon/PEDOT electrode and $C_{12}T_{add}$.[35] These implied that coating of PEDOT on carbon nanoparticles provided good electrocatalytic activity for disulfide reduction, leading to a higher FF in the DSSCs for improved PCE.

Typically, additives, such as TBP and $LiClO_4$, could optimize the charge transfer at the WE/electrolyte interface *via* suppressing the electron recombination and shifting the TiO_2 conduction band for electron injection in DSSCs to promote photovoltaic performance.[4] However, effect of the additives on liquid crystal electrolyte based DSSCs has yet to be explored. As shown in Fig. 6, $C_{12}T_{add}$ possessed a lower R_{CE} at the CE/electrolyte interface and a much smaller bulk resistance (R_b = 14 Ω cm^{-2}, derived from the Warburg impedance at the medium frequency) for efficient ion diffusion compared with $C_{12}T$ (R_b = 86 Ω cm^{-2}). These should be response for the higher J_{sc} and FF in CP-$C_{12}T_{add}$. EIS measurements of the prepared DSSCs were further conducted under dark conditions at a bias voltage of −0.6 V to analyze the effect of additives on the WE/electrolytes interface. The Nyquist plots of CP-$C_{12}T_{add}$ and CP-$C_{12}T_{add}$

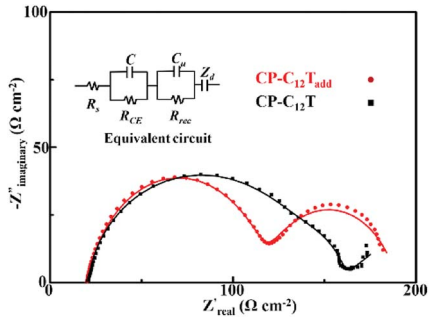

Fig. 7 Nyquist plots of the CP-$C_{12}T_{add}$ and CP-$C_{12}T$ obtained from EIS measurements at 30 °C (discrete symbols: experimental results, solid lines: fitted data, inset is the equivalent circuit).

obtained at 30 °C are shown in Fig. 7. Both the impedance spectra consisted of two semicircles and the medium frequency semicircle represented electron recombination process at the WE/electrolyte interface.[36] The recombination resistance (R_{rec}) could be extracted by fitting the equivalent circuit to the measured spectrum and higher R_{rec} corresponded to lower recombination rate, which is beneficial to photovoltaic performance because of the increased electron injection into the TiO_2.[2] The R_{rec} of CP-$C_{12}T_{add}$ (51 Ω cm^{-2}) was much higher than that of CP-$C_{12}T$ (22 Ω cm^{-2}), which suggested that the doped additives impeded the unfavored electron recombination, leading to the higher V_{oc} of CP-$C_{12}T$. These EIS measurement results indicated that doping of the additives in the liquid crystal electrolyte favored the overall charge transfer process in DSSC, which improved the FF, V_{oc} and J_{sc} of the T^-/T_2 liquid crystal electrolyte based DSSC.

4. Conclusions

A TBP and $LiClO_4$ doped lamellar nanostructured smectic electrolyte based on thiolate/disulfide redox couple and a carbon/PEDOT composite nanoparticle electrode were prepared for optimizing the photovoltaic performance of DSSCs. The introduction of the additives in the lamellar thiolate/disulfide nanostructures lowered the viscosity of the electrolyte and improved the overall charge transfer process in the DSSC. The composite nanoparticle CE provided good catalytic activity and large surface area charge transfer at the CE/electrolyte interface. As a result, the FF, J_{sc} and V_{oc} of the DSSC employing the optimized smectic thiolate/disulfide electrolyte and the composite electrode were greatly enhanced and an improved PCE value of 6.5% was obtained at 40 °C under simulated AM1.5G solar light. Notably, the derived DSSC maintained stable photovoltaic performance with PCE higher than 6.0% within a temperature range from 35 to 55 °C, which shows great potential of the organic liquid crystal electrolytes based DSSCs towards practical application.

Conflicts of interest

There are no conflicts to declare.

Acknowledgements

This work was supported by the National Natural Science Foundation of China (No. 21805199).

Notes and references

1 B. O'Regan and M. Grätzel, *Nature*, 1991, **353**, 737.
2 A. Hagfeldt, G. Boschloo, L. Sun, L. Kloo and H. Pettersson, *Chem. Rev.*, 2010, **110**, 6595.
3 S. Mathew, A. Yella, P. Gao, R. Humphry-Baker, B. Curchod, N. Ashari-Astani, I. Tavernelli, U. Rothlisberger, M. Nazeeruddin and M. Grätzel, *Nat. Chem.*, 2014, **6**, 242.
4 J. Wu, Z. Lan, J. Lin, M. Huang, Y. Huang, L. Fan and G. Luo, *Chem. Rev.*, 2015, **115**, 2136.
5 Q. Yu, Y. Wang, Z. Yi, N. Zu, J. Zhang, M. Zhang and P. Wang, *ACS Nano*, 2010, **4**, 6032.
6 A. Yella, H. Lee, H. Tsao, C. Yi, A. Chandiran, M. Nazeeruddin, E. Diau, C. Yeh, S. Zakeeruddin and M. Grätzel, *Science*, 2011, **334**, 629.
7 A. Lennert, M. Sternberg, K. Meyer, R. Costa and D. Guldi, *ACS Appl. Mater. Interfaces*, 2017, **9**, 33437.
8 Z. Zhang, P. Chen, T. Murakami, S. Zakeeruddin and M. Grätzel, *Adv. Funct. Mater.*, 2008, **18**, 341.
9 M. Wang, N. Chamberland, L. Breau, J. Moser, R. Humphry-Baker, B. Marsan, S. Zakeeruddin and M. Grätzel, *Nat. Chem.*, 2010, **2**, 385.
10 X. Xu, K. Cao, D. Huang, Y. Shen and M. Wang, *J. Phys. Chem. C*, 2012, **116**, 25233.
11 J. Liu, X. Yang, J. Cong, L. Kloo and L. Sun, *Phys. Chem. Chem. Phys.*, 2012, **14**, 11592.
12 K. Goossens, K. Lava, C. Bielawski and K. Binnemans, *Chem. Rev.*, 2016, **116**, 4643.
13 N. Yamanaka, R. Kawano, W. Kubo, T. Kitamura, Y. Wada, M. Watanabe and S. Yanagida, *Chem. Commun.*, 2005, 740.
14 R. Costa, F. Werner, X. Wang, P. Grönninger, S. Feihl, F. Kohler, P. Wasserscheid, S. Hibler, R. Beranek, K. Meyer and D. Guldi, *Adv. Energy Mater.*, 2013, **3**, 657.
15 D. Högberg, B. Soberats, S. Uchida, M. Yoshio, L. Kloo, H. Segawa and T. Kato, *Chem. Mater.*, 2014, **26**, 6496.
16 S. Tan, Z. Zhao, C. Wang and Y. Wu, *Electrochim. Acta*, 2018, **288**, 165.
17 Y. Zhu, H. Guo, H. Zheng, Y. Lin, C. Gao, Q. Han and M. Wu, *Nano Energy*, 2016, **21**, 1.
18 A. Hilmi, T. Shoker and T. Ghaddar, *ACS Appl. Mater. Interfaces*, 2014, **6**, 8744.
19 H. Wu, Z. Lv, S. Hou, X. Cai, D. Wang, H. Kafafy, Y. Fu, C. Zhang, Z. Chu and D. Zou, *J. Power Sources*, 2013, **221**, 328.
20 J. Zhang, H. Long, S. Miralles, J. Bisquert, F. Fabregat-Santiago and M. Zhang, *Phys. Chem. Chem. Phys.*, 2012, **14**, 7131.
21 H. Wu, Z. Lv, Z. Chu, D. Wang, S. Hou and D. Zou, *J. Mater. Chem.*, 2011, **21**, 14815.
22 G. Liu, X. Li, H. Wang, Y. Rong, Z. Ku, M. Xu, L. Liu, M. Hu, Y. Yang and H. Han, *Carbon*, 2013, **53**, 11.
23 H. Tian, Z. Yu, A. Hagfeldt, L. Kloo and L. Sun, *J. Am. Chem. Soc.*, 2011, **133**, 9413.

24 H. Tian, E. Gabrielsson, Z. Yu, A. Hagfeldt, L. Kloo and L. Sun, *Chem. Commun.*, 2011, **47**, 10124.
25 J. Burschka, V. Brault, S. Ahmad, L. Breau, M. Nazeeruddin, B. Marsan, S. Zakeeruddin and M. Grätzel, *Energy Environ. Sci.*, 2012, **5**, 6089.
26 K. Meng and K. Thampi, *ACS Appl. Mater. Interfaces*, 2014, **6**, 20768.
27 J. Theerthagiri, R. Senthil, M. Buraidah, J. Madhavan, A. Arof and M. Ashokkumar, *J. Mater. Chem. A*, 2016, **4**, 16119.
28 J. Theerthagiri, R. Senthil, P. Arunachalam, K. Bhabu, A. Selvi, J. Madhavan, K. Murugan and A. Arof, *Ionics*, 2017, **23**, 1017.
29 Y. Zhang, Z. Sun, C. Shi and F. Yan, *RSC Adv.*, 2016, **6**, 70460.
30 M. Berginc, U. Krašovec, M. Jankovec and M. Topič, *Sol. Energy Mater. Sol. Cells*, 2007, **91**, 821.
31 J. Wu, Z. Lan, J. Lin, M. Huang, Y. Huang, L. Fan, G. Luo, Y. Lin, Y. Xie and Y. Wei, *Chem. Soc. Rev.*, 2017, **46**, 5975.
32 J. Chen, H. Wei and K. Ho, *Sol. Energy Mater. Sol. Cells*, 2007, **91**, 1472.
33 S. Raga and F. Fabregat-Santiago, *Phys. Chem. Chem. Phys.*, 2013, **15**, 2328.
34 T. Wei, C. Wan, Y. Wang, C. Chen and H. Shiu, *J. Phys. Chem. C*, 2007, **111**, 4847.
35 F. Hao, Z. Wang, Q. Luo, J. Lou, J. Li, J. Wang, S. Fan, K. Jiang and H. Lin, *J. Mater. Chem.*, 2012, **22**, 22756.
36 Z. Xu, X. Yin, Y. Guo, Y. Pu and M. He, *J. Mater. Chem. C*, 2018, **6**, 4746.